First-principles calculations of spin spirals in Ni_2MnGa and Ni_2MnAl

J. Enkovaara,[1,*] A. Ayuela,[1] J. Jalkanen,[1] L. Nordström,[2] and R. M. Nieminen[1]
[1]*Laboratory of Physics, Helsinki University of Technology, P.O.B. 1100, FIN-02015 HUT, Finland*
[2]*Condensed Matter Theory, Department of Physics, Uppsala University, Box 530, 75121, Uppsala, Sweden*
(Received 22 October 2002; published 27 February 2003)

We report here noncollinear magnetic configurations in the Heusler alloys Ni_2MnGa and Ni_2MnAl which are interesting in the context of the magnetic shape memory effect. The total energies for different spin spirals are calculated and the ground-state magnetic structures are identified. The calculated dispersion curves are used to estimate the Curie temperature which is found to be in good agreement with experiments. In addition, the variation of the magnetic moment as a function of the spiral structure is studied. Most of the variation is associated with Ni, and symmetry constraints relevant for the magnetization are identified. Based on the calculated results, the effect of the constituent atoms in determining the Curie temperature is discussed.

DOI: 10.1103/PhysRevB.67.054417 PACS number(s): 75.30.Ds

I. INTRODUCTION

Materials showing strong coupling between the magnetic and structural properties are interesting from a technological point of view. Tb-Dy-Fe alloys (Terfenol-D, already in commercial use) exhibit magnetic-field-induced strains of $\sim 0.1\%$ based on the magnetostriction phenomenon.[1] On the other hand, Ni-Mn-Ga alloys close to the Ni_2MnGa stoichiometry show strains up to 10% with moderate magnetic fields.[2–4] The mechanism of this phenomenon, the magnetic shape memory (MSM) effect, is based on the magnetic-field-induced movement of structural domains (twin variants) and is different from ordinary magnetostriction.[5] The basic magnetic properties related to the MSM effect include the saturation magnetic moment and the magnetic anisotropy which have been studied earlier for Ni_2MnGa.[6,7] Here, we probe deeper into the magnetic properties of Ni_2MnGa and another MSM candidate, Ni_2MnAl, by studying noncollinear magnetic configurations which also enables one to consider finite-temperature effects in a natural way.

Although one ingredient in the MSM effect is a structural transformation (martensitic transformation) from a cubic structure to a lower-symmetry structure upon cooling, we concentrate here only on the high-temperature phase. In this phase Ni_2MnGa has the cubic $L2_1$ structure (see Fig. 1) as shown by *x*-ray and neutron-diffraction measurements.[8,9] The magnetic order is ferromagnetic and most of the magnetic moment originates from Mn.[9,6] In the stoichiometric compound the Curie temperature is about 370 K (Ref. 9) and decreases with increasing Ni content.[10] On the other hand, Ni_2MnAl is less studied and its structure and magnetic configuration do not seem to be perfectly understood. On the structural side, both $L2_1$ and disordered $B2$ structures are reported[11–15] depending on the thermal treatment. The magnetic configuration is found to be ferromagnetic with Curie temperatures between 300 K and 400 K in Ref. 13 and antiferromagnetic or spiral in Refs. 11 and 12. The magnetic moment comes mainly from Mn atoms also in this compound.[11,16] It seems that the ground-state magnetic configuration depends on the underlying crystal structure. Here we address the possibility of noncollinear magnetic configurations in the $L2_1$ structure.

Although the original formulation of the local-spin-density approximation[17] of density-functional theory allowed noncollinear magnetic order, first-principles calculations for this aspect have begin only recently (for a review, see Ref. 18). One application has been the study of noncollinear ground states, for example, in γ-Fe (Refs. 19–21) or in frustrated antiferromagnets.[22,23] In addition, the noncollinear formulation enables studies of finite-temperature properties of magnetic materials. Since the dominant magnetic excitations at low temperatures are spin waves which are noncollinear by nature, it is possible to determine the magnon spectra and ultimately the Curie temperature from first principles.[24–27] Most of the previous work has been done for elements or compounds with only one magnetic constituent. We study here systems with several magnetic atoms and show how the interaction between different magnetic sublattices can give rise to interesting effects.

The paper is organized as follows. Some general properties of spin spirals are discussed in Sec. II followed by the description of the computational scheme in Sec. III. We study the total energy and magnetization with spiral mag-

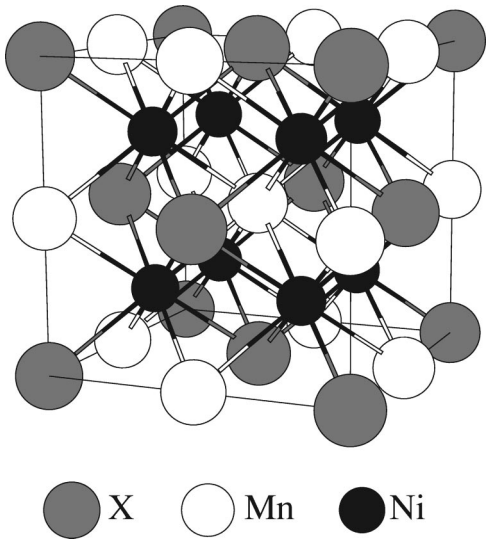

FIG. 1. Cubic cell of the $L2_1$ structure, where *X* is Al or Ga. The cubic cell contains four primitive cells.

netic orderings and estimate the Curie temperature in Sec. IV and finally we conclude in Sec. V.

II. GENERAL PROPERTIES OF SPIN SPIRALS

The magnetic configuration of an incommensurate spin spiral shows the magnetic moments of certain atomic planes varying in direction. The variation has a well-defined period determined by a wave vector $\boldsymbol{q}$. When the magnetic moment is confined to the lattice sites the magnetization $\boldsymbol{M}$ varies as

$$\boldsymbol{M}(\boldsymbol{r}_n) = m_n \begin{bmatrix} \cos(\boldsymbol{q}\cdot\boldsymbol{r}_n + \phi_n)\sin(\theta_n) \\ \sin(\boldsymbol{q}\cdot\boldsymbol{r}_n + \phi_n)\sin(\theta_n) \\ \cos(\theta_n) \end{bmatrix}, \tag{1}$$

where polar coordinates are used and m_n is the magnetic moment of atom n with a phase ϕ_n at the position $\boldsymbol{r}_n$. Here, we consider only planar spirals, that is, $\theta_n = \pi/2$ which also gives the minimum of the total energy. When the spin-orbit interaction is neglected the z directions in spin space and real space are not coupled and the relative orientations of the magnetic moments are the important quantities. The magnetization of Eq. (1) is not translationally invariant but transforms as

$$\boldsymbol{M}(\boldsymbol{r}+\boldsymbol{R}) = D(\boldsymbol{q}\cdot\boldsymbol{R})\boldsymbol{M}(\boldsymbol{r}), \tag{2}$$

where $\boldsymbol{R}$ is a lattice translation and D is a rotation around the z axis. A spin spiral with a magnetization in a general point $\boldsymbol{r}$ in space can be defined as a magnetic configuration which transforms according to Eq. (2). Since the spin spiral describes a spatially rotating magnetization, it can be correlated with a frozen magnon.

Because the spin spiral breaks translational symmetry, the Bloch theorem is no longer valid. Computationally, one should use large supercells to obtain total-energy spin spirals. However, one can define generalized translations which contain translations in real space and rotations in spin space.[28,29] These generalized translations leave the magnetic structure invariant and lead to a generalized Bloch theorem. Therefore the Bloch spinors can still be characterized by a $\boldsymbol{k}$ vector in the Brillouin zone, and can be written as

$$\psi_k(\boldsymbol{r}) = e^{i\boldsymbol{k}\cdot\boldsymbol{r}} \begin{pmatrix} e^{-i\boldsymbol{q}\cdot\boldsymbol{r}/2}u_k(\boldsymbol{r}) \\ e^{+i\boldsymbol{q}\cdot\boldsymbol{r}/2}d_k(\boldsymbol{r}) \end{pmatrix}. \tag{3}$$

The functions $u_k(\boldsymbol{r})$ and $d_k(\boldsymbol{r})$ are invariant with respect to lattice translations having the same role as for normal Bloch functions. Due to this generalized Bloch theorem the spin spirals can be studied within the chemical unit cell and no large supercells are needed.

Although the chemical unit cell can be used, the presence of the spin spiral lowers the symmetry of the system. Only the space-group operations that leave invariant the wave vector of the spiral remain. When considering the general spin space groups, i.e., taking the spin rotations into account, the space-group operations which reverse the spiral vector together with a spin rotation of π around the x axis are symmetry operations.[29]

Basically, the spin spiral relates only the magnetizations in the different primitive cells. However, the symmetry properties constrain the magnetization which we discuss here in the context of the $L2_1$ structure. The primitive cell of the $L2_1$ structure (one-fourth of the cubic cell shown in Fig. 1) contains four atoms: two Ni, one Mn, and one Ga or Al atom. In the full cubic symmetry the two Ni atoms are equivalent but this equivalence can be broken when the spin spiral lowers the symmetry of the system. If the spiral wave vector is in the [111] direction the two Ni atoms are no longer equivalent under space-group operations. Considering also the spin rotations, the phases ϕ_n of the two Ni magnetizations are opposite since the atoms are related by space inversion. If the two Ni atoms are treated as equivalent (when allowed by the spiral symmetry) constraints for the phases of Ni moments are even stronger. If the magnetic moments of Ni within the primitive cell are $\boldsymbol{M}(\boldsymbol{r}_1) = m_1\cos(\phi_1) = \boldsymbol{M}(\boldsymbol{r}_2)$, the magnetic moment in the neighboring cell at $-\boldsymbol{r}_1$ is $\boldsymbol{M}(-\boldsymbol{r}_1) = m_1\cos(-\phi_1)$. On the other hand, the Ni atoms at $-\boldsymbol{r}_1$ and at $\boldsymbol{r}_2$ are connected by a lattice translation, so that according to Eq. (2) $\boldsymbol{M}(\boldsymbol{r}_2) = m_1\cos(-\phi_1 + \boldsymbol{q}\cdot\boldsymbol{R})$ and one has the relation $\phi_1 = -\phi_1 + \boldsymbol{q}\cdot\boldsymbol{R}$ for the phase. In order to obtain the true minimum-energy configuration it may be necessary to treat the Ni atoms as inequivalent (i.e., lower the symmetry of the system) so that the above relation for the phase does not have to hold.

III. COMPUTATIONAL METHOD

The spin spirals discussed in Sec. II are studied within density-functional theory. We use the full-potential linearized augmented-plane-wave method[30] in an implementation which allows noncollinear magnetism including spin spirals.[31,32] In addition to the full charge density and to the full potential, the full magnetization density is used. The magnetic moment is allowed to vary both in magnitude and in direction inside the atomic spheres as well as in the interstitial regions. The plane-wave cutoff for the basis functions is $RK_{max} = 9$, leading to ~ 350 plane waves with muffin-tin radii of 2.25 a.u. Brillouin-zone integrations are carried out with the special point method using 800 k points in the full Brillouin zone and a Fermi broadening of 0.005 Ry. Total energies are given per formula unit and they are converged at least up to 0.01 mRy. For the exchange-correlation potential we use both the local-spin-density approximation[17] (LSDA) and the generalized gradient approximation (GGA),[33] which we discuss next in more detail.

A. LSDA vs GGA

It has been pointed out that the use of the GGA is beneficial in the context of Ni_2MnGa.[16,6] Because there has been some discussion about the different exchange-correlation potentials in the context of noncollinear magnetism, we present some comparison also here.

Although there is no global spin-quantization axis, one can consider at every point of space a local coordinate system such that the magnetization at that point is in the z direction. Since the LSDA depends only on the magnitude of

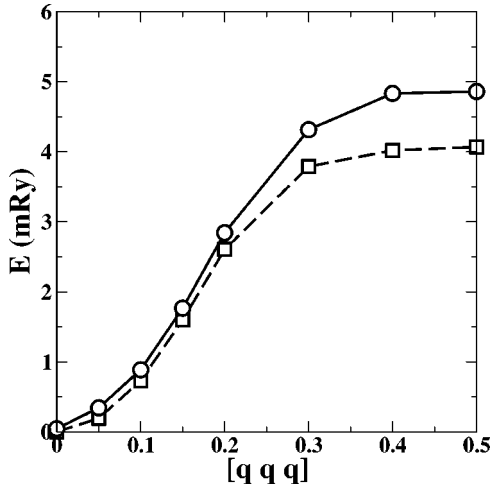

FIG. 2. Total energy as a function of the spiral vector $\boldsymbol{q}$ in units of $2\pi/a$. Circles represent LSDA, squares are for GGA.

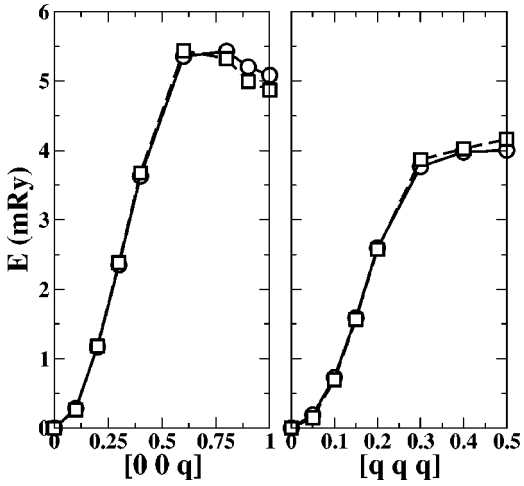

FIG. 3. Total energy as a function of the spiral vector $\boldsymbol{q}$. Circles represent Ni_2MnAl, squares are for Ni_2MnGa.

the magnetization, the exchange-correlation potential can be calculated at every point in the local coordinate system such as in the usual collinear case. The noncollinear potential is obtained by rotating back to the global frame of reference. On the other hand, the GGA depends also on the gradients of magnetization. Because the magnetization direction may vary, only projections of the magnetization on the local quantization axis are used in the standard GGA when evaluating the gradients. If the magnetization direction varies slowly this should not cause any problems. Some previous work has led to suggestions that the disagreements between theory and experiment are due to projection errors in some cases.[20] However, later work has corroborated the fact that the main issue is not the exchange-correlation functional but the actual computational method, pointing to the importance of all-electron and full-magnetization treatments.[21,34,35]

We have done all the calculations in this work both with the LSDA and the GGA. The total energy as a function of the spiral wave-vector length in Ni_2MnGa is shown in Fig. 2 for a single direction.

One can see that for small q both approximations give similar results. With larger q the results differ slightly but the same qualitative behavior is seen. For the other results presented in the following sections the qualitative behavior is also the same for the LSDA and GGA, and the quantitative differences between the two approximations are even smaller. The differences between the LSDA and GGA in spin spiral calculations are small also for pure elements.[21] Therefore, only the GGA results are discussed in the following.

IV. RESULTS AND DISCUSSION

A. Total energies

First, we have studied the possibility of noncollinear ordering by studying the energetics of spiral configurations. This study also provides information about finite-temperature properties. The total energy is calculated as a function of the spiral wave vector $\boldsymbol{q}$, and the wave vector is varied along the high-symmetry directions [001], [110], and [111]. $\boldsymbol{q}$ is given in units of $2\pi/a$ where a is the theoretical lattice constant of the $L2_1$ structure.[16] The corresponding total energies are shown in Figs. 3 and 4.

Figure 3 shows that the variation of total energy in [001] and [111] directions is similar in Ni_2MnGa and Ni_2MnAl for all values of $\boldsymbol{q}$. The lowest energy in all cases is at $q=0$ which is the normal collinear ferromagnetic configuration. Both materials have small minima at the antiferromagnetic configuration at $\boldsymbol{q}=(0\,0\,1)$, but at other antiferromagnetic configurations at $\boldsymbol{q}=(0.5\,0.5\,0.5)$ there are no minima.

The energy in the [110] direction is also similar for both materials as seen in Fig. 4. Here, the effect of symmetry constraints can be seen clearly. If the two Ni atoms are equivalent the energy is higher especially around $\boldsymbol{q}=(0.5\,0.5\,0)$. When the magnetic moments of the two Ni are allowed to relax independently the energy lowers and the dispersion becomes flat after $\boldsymbol{q}=(0.5\,0.5\,0)$. Near the Brillouin-zone boundary at $\boldsymbol{q}=(0.75\,0.75\,0)$ both materials

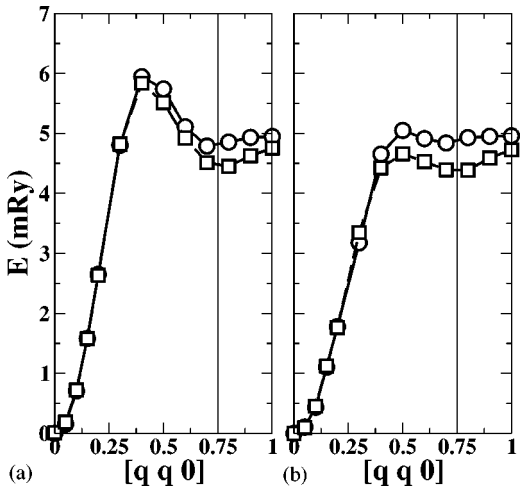

FIG. 4. Total energy as a function of the spiral vector $\boldsymbol{q}$. Circles represent Ni_2MnAl, squares are for Ni_2MnGa. (a) Ni atoms are equivalent; (b) Ni atoms are inequivalent. Vertical line denotes the Brillouin-zone boundary.

show small energy minima corresponding to incommensurate spiral order. At the antiferromagnetic configurations at $\boldsymbol{q}=(1\,1\,0)$ there are no clear energy minima even though in the case of Ni_2MnAl the dispersion is very flat.

Generally, the spin spirals are related to magnons which allows the estimation of magnon-related properties, such as spin stiffness and Curie temperature, from the total energies calculated above. The total energy of the planar spin spiral is related to the magnon energy ω_q as[24,26]

$$\omega_q = \frac{4\mu_B}{M} E(\boldsymbol{q}), \tag{4}$$

where M is the magnetic moment per unit cell. In the low-q limit the magnon dispersion is quadratic, and one defines the spin stiffness constant D as

$$\omega_q = Dq^2. \tag{5}$$

From the calculated total energies in Figs. 3 and 4 we can estimate the same spin stiffness for both materials which is $D=77$ mRy a.u.^{2} This in good agreement with the experimental value 79 mRy a.u.^{2} measured in Ni-Mn-Ga films.[36]

The Curie temperature can be estimated on the basis of the Heisenberg model. By mapping the first-principles results to the Heisenberg model, the Curie temperature T_c in the random-phase approximation is given by[27,37]

$$\frac{1}{k_B T_C} = \frac{6\mu_B}{M} \frac{V}{(2\pi)^3} \int d^3q \frac{1}{\omega_q}, \tag{6}$$

where V is the unit-cell volume, and the integration is over the Brillouin zone. An estimation can be obtained using the quadratic dispersion, Eq. (5), and carrying out the integration over a sphere having the same volume as the Brillouin zone. This results in

$$\frac{1}{k_B T_C} = \frac{3Vq_d}{M\pi^2 D}, \tag{7}$$

where $q_d=(6\pi^2/V)^{1/3}$. By using the calculated spin stiffness constant we obtain $T_c=830$ K which is clearly an overestimate. As seen in Figs. 3 and 4 the dispersion curve $E(\boldsymbol{q})$ deviates strongly from quadratic behavior with larger q. A better estimate can be obtained by considering the dispersion quadratic up to some radius and constant thereafter. Based on the calculated energies in Figs. 3 and 4 the constant is chosen to be 5 mRy when $q>0.7q_d$. The Curie temperature obtained in this way is $T_c=485$ K which compares well with the experimental one, 380 K.

B. Magnetic moments

In order to obtain a deeper understanding of the energy dispersion we next look into the behavior of magnetization. The magnetic moments averaged over the atomic spheres for different $\boldsymbol{q}$ are shown in Figs. 5 and 6. The atomic magnetizations show that within the Mn spheres the magnetization is nearly constant and the variation in the total magnetization is mainly due to Ni. Also, the symmetry consideration of the

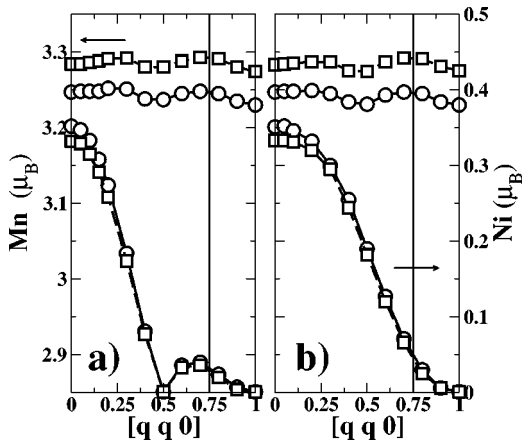

FIG. 5. Magnetic moments within the atomic spheres as a function of the spiral vector $\boldsymbol{q}$. Circles represent Ni_2MnAl, squares are for Ni_2MnGa. (a) Ni atoms are equivalent; (b) Ni atoms are inequivalent.

equivalence of Ni atoms has no effect on the Mn moment. This points to a more localized character of the magnetic moment of Mn, compared to a more itinerant character of Ni. Because most of the total magnetic moment comes from Mn, these alloys can be considered as localized-moment systems consistent with the traditional view for similar materials.[38] However, despite the relative smallness of its magnetic moment, Ni has a significant effect on the energetics as discussed later. The differences between Ni_2MnGa and Ni_2MnAl are small: the magnetic moment in Ni_2MnGa is slightly larger, as shown already in previous work.[16]

Since the magnetic moment in Ni shows a larger variation, the behavior of the Ni moment for several directions is analyzed in more detail. The magnetization decreases monotonously both in the [001] and in the [111] directions. Differences are at the antiferromagnetic configurations since the magnetic moment of Ni remains finite at $\boldsymbol{q}=(1\,1\,1)$ but vanishes at $\boldsymbol{q}=(0\,0\,1)$. In the [110] direction, the behavior of the Ni moment depends strongly on the symmetry as seen

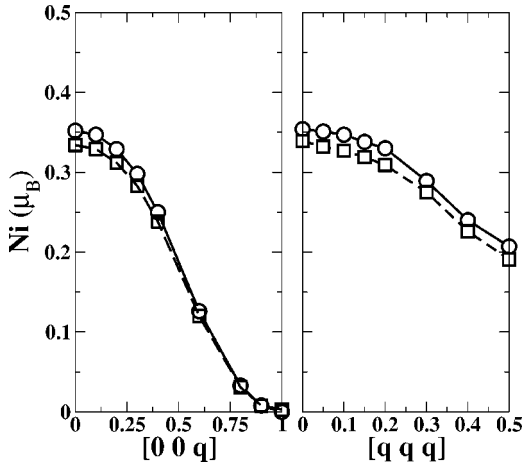

FIG. 6. Magnetic moments within the Ni sphere as a function of the spiral vector $\boldsymbol{q}$. Circles represent Ni_2MnAl, squares are for Ni_2MnGa.

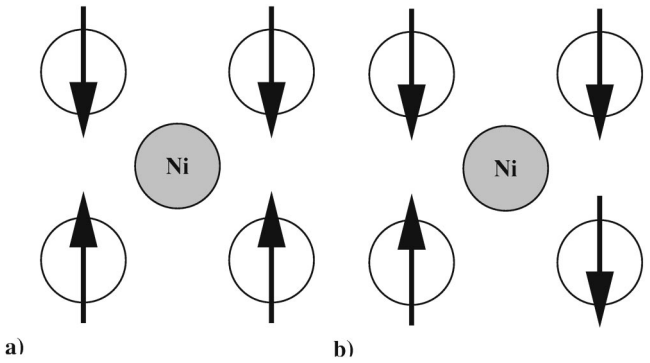

FIG. 7. Schematic view of magnetic moments in nearest-neighbor Mn atoms of Ni atoms at (a) $\boldsymbol{q}=(0\,0\,1)$ and (b) $\boldsymbol{q}=(0.5\,0.5\,0.5)$.

in Fig. 5. When the two magnetic moments are forced to be the same, the magnetization starts to decrease with increasing q and vanishes to zero value at $\boldsymbol{q}=(0.5\,0.5\,0)$. For larger q values the moment shows a small peak before decreasing again to zero in the antiferromagnetic state at $\boldsymbol{q}=(1\,1\,0)$. In the case of Ni atoms being inequivalent only a monotonous decrease similar to the [001] direction is seen.

Because most of the variation in total magnetization is due to Ni, it should have a stronger effect also on the energy dispersion. The importance of Ni can be seen most clearly in the [110] direction for the cases of different symmetry. The symmetry affects only Ni as seen in the behavior of the magnetization, Fig. 5. Since the energy dispersion depends on the symmetry, Fig. 4, the importance of Ni is clear. Comparison of Figs. 5 and 4 shows that the energy lowers when the Ni moment increases. Based on the above reasoning, Ni should have an effect on the Curie temperature, which indeed is seen in experiments where the increase in Ni content decreases the Curie temperature.[10]

The variation of the Ni moment can be understood by considering symmetry arguments and the coordination around Ni atoms. In the [001] direction two of the four Mn atoms neighboring Ni have the same magnetization direction in the spiral and the other two have different directions, as shown schematically in Fig. 7(a). The magnetization in Ni favors ferromagnetic alignment with the neighboring Mn moments so that part of the Ni moment can be thought to align with one group of the Mn neighbors and part with the other group. The total moment within the atomic sphere is an average of these two parts and the Ni moment decreases when the angle between the Mn moments increases. In the antiferromagnetic configuration there is a complete frustration of the Ni atoms which results in a zero average magnetization within the sphere. For the [111] direction shown in Fig. 7(b) one group contains three Mn atoms and the other group only one. Therefore the variation of the average moment in the Ni sphere is smaller and the moment remains finite in the antiferromagnetic configuration.

In the [110] direction the situation is more complex especially when the two Ni atoms are treated as equivalent. In the antiferromagnetic configuration the coordination is similar to the case of the [001] direction. There are two groups of neighboring Mn atoms with antiparallel magnetization, and

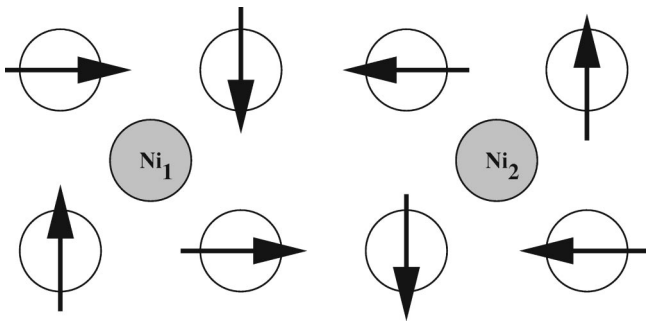

FIG. 8. Schematic view of magnetic moments in nearest-neighbor Mn atoms of the two equivalent Ni atoms at $\boldsymbol{q}=(0.5\,0.5\,0)$.

the frustration leads to a zero average moment within the Ni sphere. The Ni moment is, however, zero also at $\boldsymbol{q}=(0.5\,0.5\,0)$. At this point there are three groups of equivalent Mn neighbors. One group contains two Mn atoms and the other groups contain one Mn atom. The magnetic moments of single Mn atoms are antiparallel to each other and have a 90° angle with respect to the moments in the group of the two Mn atoms. The other equivalent Ni atom has three similar groups of neighboring Mn atoms, such as the first Ni atom. The important point is that the moments in the group with two Mn atoms are antiparallel to those in the corresponding group of the first Ni atom, as seen in Fig. 8. There is now frustration for Ni, but only when both equivalent Ni atoms and their neighbors are taken into account. This frustration causes the magnetic moment around Ni to vanish completely in contrast to the antiferromagnetic case, where a small moment remains near Ni but averages to zero. When the Ni atoms are inequivalent, they can relax according the local environment so that a finite moment can remain at $\boldsymbol{q}=(0.5\,0.5\,0)$.

An example of the magnetization density for the case in which finite magnetic moments near the Ni atom average to zero is seen in Fig. 9. Here the magnetization direction can change its sign within the atomic sphere. This finding shows the importance of the full-magnetization treatment when dealing with several magnetic sublattices.

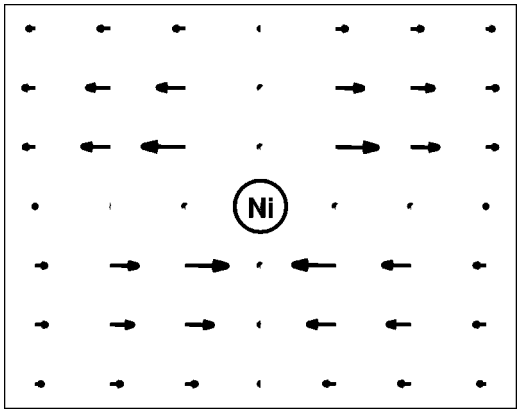

FIG. 9. Magnetization density around Ni in the (001) plane with $\boldsymbol{q}=(1\,1\,0)$. The width and the height of the area are 2.5 a.u. while magnetization is in arbitrary units.

V. CONCLUSIONS

We have studied noncollinear magnetic configurations in the ternary alloys Ni_2MnGa and Ni_2MnAl with first-principles calculations. The calculations show that the magnetic properties are similar for both materials. The ferromagnetic configuration is the ground state in the $L2_1$ structure, so that the experimentally observed antiferromagnetism of Ni_2MnAl is related to structural disorder. Studies of the other structural phases as well as inner distortions would be interesting in the future.

The calculated total energies are used to estimate the spin stiffness constant and the Curie temperature, which are in good agreement with the experiments. The similarity in the energy dispersion for both materials suggests that the Curie temperatures should be also similar. In the [110] direction Ni_2MnAl has higher energy, so that the Curie temperature should be slightly higher.

The variation of the magnetic moment in the spirals shows that the Mn moment is nearly constant while the Ni moment varies strongly. The symmetry of the spin spiral constrains the direction of magnetization, and since Ni favors ferromagnetic coupling with Mn, there can be frustration at certain wave vectors resulting in the vanishing of the magnetic moment near the Ni sites. It is also shown how there can be strong variation in the direction of the magnetization near the atomic sites which points to the relevance of the full-magnetization treatment.

Some conclusions can be made concerning the role of the constituent atoms for the magnetic properties. Since the magnetic moment of Ni varies strongly and its symmetry affects the energy considerably, Ni has probably a strong effect on the energy dispersion especially when larger wave vectors are involved. Therefore Ni also influences the Curie temperature. If one assumes that the spin stiffness is mainly due to Mn, and the lowering of the energy with larger wave vectors due to Ni, Ni lowers the Curie temperature from 830 K to 485 K within the present approximations. Since the increase in the Ni moment decreases the energy it is suggested that in order to increase the Curie temperature one should replace some Ni, perhaps a little counterintuitively, with some nonmagnetic element, for example, Cu. Further experiments should clarify these issues and confirm the above suggestions.

ACKNOWLEDGMENTS

This work was supported by the Academy of Finland (Centers of Excellence Program 2000–2005), by the National Technology Agency of Finland (TEKES), and the consortium of Finnish companies (ABB Corporate Research Oy, AdaptaMat Oy, Metso Oyj, Outokumpu Research Oy). A. Ayuela was supported by the EU TMR program (Contract No. ERB4001GT954586). Computer facilities of the Center for Scientific Computing (CSC), Finland, are greatly acknowledged. L. N. acknowledges the support from the Swedish Research Council and the Swedish Foundation for Strategic Research.

*Electronic address: jen@fyslab.hut.fi

[1] A.E. Clark, in *Ferromagnetic Materials*, edited by E. P. Wohlfarth (North-Holland, Amsterdam, 1980), Vol. 1, p. 531.
[2] S.J. Murray, M. Marioni, S.M. Allen, R.C. O'Handley, and T.A. Lograsso, Appl. Phys. Lett. **77**, 886 (2000).
[3] O. Heczko, A. Sozinov, and K. Ullakko, IEEE Trans. Magn. **36**, 3266 (2000).
[4] A. Sozinov, A.A. Likhachev, N. Lanska, and K. Ullakko, Appl. Phys. Lett. **80**, 1746 (2002).
[5] R.J. James and K.F. Hane, Acta Mater. **48**, 197 (2000).
[6] A. Ayuela, J. Enkovaara, and R.M. Nieminen, J. Phys.: Condens. Matter **14**, 5325 (2002).
[7] J. Enkovaara, A. Ayuela, L. Nordström, and R.M. Nieminen, Phys. Rev. B **65**, 134422 (2002).
[8] P.J. Webster, Contemp. Phys. **10**, 559 (1969).
[9] P.J. Webster, K.R.A. Ziebeck, S.L. Town, and M.S. Peak, Philos. Mag. B **49**, 295 (1984).
[10] A.N. Vasil'ev, A.D. Bozhko, V.V. Khovailo, I.E. Dikshtein, V.G. Shavrov, V.D. Buchelnikov, M. Matsumoto, S. Suzuki, T. Takagi, and J. Tani, Phys. Rev. B **59**, 1113 (1999).
[11] K.R.A. Ziebeck and P.J. Webster, J. Phys. F: Met. Phys. **5**, 1756 (1975).
[12] S. Morito, T. Kakeshita, K. Hirata, and K. Otsuka, Acta Mater. **46**, 5377 (1998).
[13] A. Fujita, K. Fukamichi, F. Gejima, R. Kainuma, and K. Ishida, Appl. Phys. Lett. **77**, 3054 (2000).
[14] M. Acet, E. Duman, E.F. Wassermann, L. Mañosa, and A. Planes, J. Appl. Phys. **92**, 3867 (2002).
[15] L. Mañosa, A. Planes, M. Acet, E. Duman, and E. F. Wassermann (unpublished).
[16] A. Ayuela, J. Enkovaara, K. Ullakko, and R.M. Nieminen, J. Phys.: Condens. Matter **11**, 2017 (1999).
[17] U. von Barth and L. Hedin, J. Phys. C **5**, 1629 (1972).
[18] L.M. Sandratskii, Adv. Phys. **47**, 91 (1998).
[19] L.M. Sandratskii and J. Kübler, J. Phys.: Condens. Matter **4**, 6927 (1992).
[20] D.M. Bylander and L. Kleinman, Phys. Rev. B **59**, 6278 (1999).
[21] K. Knöpfle, L.M. Sandratskii, and J. Kübler, Phys. Rev. B **62**, 5564 (2000).
[22] P. Kurz, G. Bihlmayer, K. Hirai, and S. Blügel, Phys. Rev. Lett. **86**, 1106 (2001).
[23] D. Hobbs and J. Hafner, J. Phys.: Condens. Matter **12**, 7025 (2000).
[24] N.M. Rosengaard and B. Johansson, Phys. Rev. B **55**, 14 975 (1997).
[25] M. Uhl and J. Kübler, Phys. Rev. Lett. **77**, 334 (1996).
[26] S.V. Halilov, H. Eschrig, A.Y. Perlov, and P.M. Oppeneer, Phys. Rev. B **58**, 293 (1998).
[27] M. Pajda, J. Kudrnovsky, I. Turek, V. Drchal, and P. Bruno, Phys. Rev. B **64**, 174402 (2001).
[28] C. Herring, in *Magnetism*, edited by G. Rado and H. Suhl (Academic, New York, 1966), Vol. 4.
[29] L.M. Sandratskii, J. Phys.: Condens. Matter **3**, 8565 (1991).
[30] E. Wimmer, H. Krakauer, M. Weinert, and A.J. Freeman, Phys. Rev. B **24**, 864 (1981).
[31] L. Nordström and D.J. Singh, Phys. Rev. Lett. **76**, 4420 (1996).

[32] L. Nordström and A. Mavromas, Europhys. Lett. **49**, 775 (2000).
[33] J.P. Perdew and Y. Wang, Phys. Rev. B **45**, 13 244 (1992).
[34] E. Sjöstedt and L. Nordström, Phys. Rev. B **66**, 014447 (2002).
[35] M. Marsman, D. Hobbs, G. Kresse, and J. Hafner (unpublished).
[36] S.I. Patil, D. Tan, S.E. Lofland, S.M. Bhagat, I. Takeuchi, O. Famodu, J.C. Read, K.-S. Chang, C. Craciunescu, and M. Wuttig, Appl. Phys. Lett. **81**, 1279 (2002).
[37] C.S. Wang, R.E. Prange, and V. Korenman, Phys. Rev. B **25**, 5766 (1982).
[38] J. Kübler, A.R. Williams, and C.B. Sommers, Phys. Rev. B **28**, 1745 (1983).